Journal of Molecular Liquids 359 (2022) 119254

Contents lists available at ScienceDirect

Journal of Molecular Liquids

journal homepage: www.elsevier.com/locate/molliq

Optically isotropic nano-size encapsulation of nematic liquid crystals with a high-filling factor

Seok Lyul Lee [a,1], MinSu Kim [b,1], DaYeon Lee [b], Yi-Hsin Lin [a,*], Seung Hee Lee [b,*]

[a] Department of Photonics, National Yang Ming Chio Tung University, Hsinchu 30010, Taiwan
[b] Department of Nano Convergence Engineering, and Department of Polymer Nano Science and Technology, Jeonbuk National University, Jeonju, Jeonbuk 54896, Korea

ARTICLE INFO

Article history:
Received 25 January 2022
Revised 16 March 2022
Accepted 23 April 2022
Available online 28 April 2022

Keywords:
Encapsulation
Liquid crystals
Polymers
Electro-optics
Optical isotropy
LC-polymer composite system

ABSTRACT

The filling factor of LCs in the LC-polymer composite system is a crucial factor for the electro-optic performance of optically isotropic liquid crystal (OILC) devices. The polymerization-induced phase separation method is well-known method to fabricate the OILCs; however, this method spontaneously limits the filling factor by ~ 40%, which is inadequately low, owing to low-LC concentration in the mixtures. To overcome such intrinsic problem, we propose an encapsulated LC which is fabricated by means of oil-in-water encapsulation. Through this approach, the filling factor of LCs is effectively increased up to 67.8% because the capsules are closely packed. Consequently, we achieve a thin-composite film of nano-size LC encapsulation whose isotropic state is reliably switched to anisotropic state in response to an external electric field with low-operation voltage (E_{th} = 1.4 V/μm and E_{op} = 4.6 V/μm), fast-response time (τ_{on} = 0.5 ms, τ_{off} = 2.2 ms), and hysteresis-free electro-optic behavior. The highly improved electro-optic performances of the proposed encapsulated LC device would give versatile applications in blooming free-form flexible displays and various tunable photonic systems.

© 2022 Elsevier B.V. All rights reserved.

1. Introduction

Flexibility is a key feature for multifunctional applications in wearable devices, sensors, and displays. Light emitting materials such as organic light emitting diodes (OLEDs) are optically ideal for flexible displays [1,2]. Nevertheless, when we adopt non-emissive materials to modulate light, such as liquid crystals (LCs), the functionality and applicability are wide and versatile because of capability of adopting the passive optical effects, such as light scattering, diffraction, refraction, reflection, and even combination of all these. In liquid crystal displays (LCDs), LCs modulate incident polarized light via well-aligned LC molecules at pixels under applied electric fields, controlled by thin-film transistors. The optic axes of LC molecules are reoriented under applied electric fields and then the polarized incident light experiences phase retardation between extraordinary wave and ordinary wave. An LCD exhibits a change in transmission as a LC layer is placed between two polarizers. However, the geometric deformation, which is essential in flexible LCDs, always results in light leakage because of non-uniform thickness of curved LC layers, non-uniform alignment of LC molecules in curved LC layers, extra stress-induces birefringence of curved polarizers [3,4]. This all leads to poor dark states which turn out poor contrast ratio of flexible LCDs. It motivates us to develop optically isotropic LCDs whose optical polarization state is relatively independent on the geometric deformation. In prior arts, optically isotropic LCs can be achieved by means of LC-polymer composite materials [5–8]. Such optically isotropic LC-polymer composite is similar to polymer-dispersed liquid crystals (PDLCs), fabricated by the polymerization-induced phase separation, but the size of polymeric cavities or pores that contain LCs is much smaller than the wavelength of light in order to avoid light scattering and display a feature of a polarization independent optical phase modulation. However, the interactive energy of optically isotropic LC-polymer composite between the LC and the polymer is too high to harness. As a result, the concentration of LCs in the optically isotropic LC-polymer composite should be<50% to display the optical isotropy [6]. When the size of a polymeric cavity is large, the correlation length in the polymer networks is longer, which results in an increase of light scattering, especially the wavelength of incident light and the size of a polymeric cavity are compatible. This ultimately leads to low transmittance and high-driving voltages in the optically isotropic LC.

The birefringence of optically isotropic LCs (the dielectric anisotropy of LC $\Delta\varepsilon$ greater than 0 or $\Delta\varepsilon < 0$) is induced under an external stimulus, such as an applied voltage, which is known as the

* Corresponding authors.
E-mail addresses: yilin@mail.nctu.edu.tw (Y.-H. Lin), lsh1@jbnu.ac.kr (S.H. Lee).
[1] These authors equally contribute to this work.

https://doi.org/10.1016/j.molliq.2022.119254
0167-7322/© 2022 Elsevier B.V. All rights reserved.

Kerr effect [9]. When the host LC is blue phase liquid crystals (BPLCs) in LC-polymer composite materials, the induced birefringence is expressed as [10].

$$\Delta n_{ind} = \lambda K E^2 \tag{1}$$

where λ is light wavelength, K is the Kerr constant, and E is the electric field strength. In principle, an increase of Δn_{ind} by means of increasing the K and E help us not only to keep the same phase retardation at low-operating voltage, but also enhance transmittance. The field-induced birefringence in Equation (1) of optically isotropic LCs can be seen as a deformation of refractive-index ellipsoid and the optic axis of the refractive-index ellipsoid is along the direction of the electric field. Thus, the birefringence Δn of the host LC is always greater than the Δn_{ind} due to the local reorientations of the LC molecules. We can reasonably presume that the average-refractive index is a constant under various electric fields, n_{avg} = $(2n_{\mathrm{o}}(E) + n_{\mathrm{e}}(E)) / 3 = n_{\mathrm{iso}}$ where $n_{\mathrm{o}}(E)$ and $n_{\mathrm{e}}(E)$ are the field-dependent ordinary refractive index n_{o} and extraordinary refractive index n_{e} [10]. The change in refractive index between E and no electric field δn then can be described as.

$$\delta n = n_{iso} - n_o(E) = \frac{n_e(E) - n_o(E)}{3} \tag{2}$$

and the Kerr effect can be extended to fit practical measurement by considering the dependence of the high-order term at strong electric field strength and by minimizing the fourth-order term in the electro-optic effects as [11],

$$\delta n = \delta n_{sat}\left(1 - e^{\left[-\left(\frac{E}{E_{sat}}\right)^2\right]}\right) \tag{3}$$

where δn_{sat} and E_{sat} denote the saturation refractive index change and the saturation electric field. In Equation (3), the model describes the Kerr effect when the applied electric field is strong, and the refractive index change δn is closed to encounter the saturation point δn_{sat}.

Many literatures have proposed different approaches to enhance the electro-optical properties of optically isotropic LCs, including BPLCs, such as implementing wall-shape (protrusion) electrodes that promise greater contribution of the in-plane vector component for LCs to reorient [12–16] and developing materials with a large Kerr constant because the driving voltage is inversely proportional to $K^{1/2}$ [5,6,17–22]. According to the Gerber's model of BPLCs, it suggests that Kerr constant depends on birefringence Δn, dielectric anisotropy $\Delta\varepsilon$, the elastic constant K_{LC} and chiral pitch p of the host LC, and the relation should be $K \approx \frac{\Delta n \Delta\varepsilon\varepsilon_0 p^2}{\lambda K_{LC} 4\pi^2}$ [23]. In case of optically isotropic LCs, the cavity size R replaces the chiral pitch and Kerr constant is then written as,

$$K \approx \frac{\Delta n \Delta\varepsilon\varepsilon_0 R^2}{\lambda K_{LC} 4\pi^2} \tag{4}$$

However, the filling factor of LCs in optically isotropic LC-polymer composites is also a crucial factor, which is not included in Equation (4). To elucidate how filling factor affects the Kerr constant, the polymerization-induced phase separation method may not be an ideal approach to achieve a good electro-optic performance governed by the Kerr effect and Δn in Equation (4) should be modified as,

$$\Delta n = \Delta n_{composite} \approx \Delta n_{LC} c_{LC} + \Delta n_{Polymer} c_{Polymer} \tag{5}$$

where c denotes the concentration of each component (LC or polymer) in the LC-polymer composite. Therefore, to enhance the K, the filling factor of LC in the LC-polymer composite is the crucial control parameter.

For the enhancement of the filling factor of LCs, preformation of enclosed LCs could be an ideal solution because they can be closely packed after removal of solvent after coating on the surface. Many works have demonstrated the oil-in-water based approach to encapsulate LCs in water for variety of applications such as color correlative optical responses or structural color generations [17,24]. In this work, we show nano-size LC encapsulation surrounded by a polymeric shell, polyvinyl alcohol (PVA) in water to achieve the high filling factor of LCs in the LC-polymer composite system. Through this approach, we can achieve a thin-composite film of nano-size LC encapsulation whose isotropic state is reliably switched to anisotropic state in response to an external electric field. We fabricate the LCs encapsulated by PVA shells in water and blade-coat onto a single substrate with interdigitated electrodes where the size distribution of LC capsules is well controlled. The solvent water is easily dried away so that the LC filling factor is highly achieved.

Another important drawback in the optically isotropic LC is residual birefringence that causes an electro-optic hysteresis, which is reported with many approaches to solve such as controlling polymer morphology [18–20,25], polymer-stabilized amorphous BP (BPIII) [18,20,25,26], monodomain or single crystalline BPs [22,27,28] and mixing with nanoparticle additives [13–15]. However, the key reason of the residual birefringence is the high-driving voltage, which breaks both initial polymer morphology and the alignment of LCs. The LC encapsulation method achieves meaningfully low-driving voltage that does not break the initial polymer morphology and LC alignment so that no residual birefringence is generated. With the proposed nano-size LC encapsulation method, superior electro-optic properties are achieved in the experimental demonstration, compared with optically isotropic LC.

2. Experimental Section

2.1. Encapsulation in the mixtures.

We used a nematic LC ($\Delta\varepsilon$ = 18 at 1 kHz, T_{NI} = 85 °C, n_{e} = 1.752, n_{o} = 1.512, Δn = 0.24 at 589 nm, ImageLab), a partially-hydrolyzed Polyvinyl Alcohol (PVA) with an average molecular weight, 22,000 Mn, and a degree of hydrolysis of 85 % mol (Kuraray, Japan), Surfynol 420 (HLB:4.0, BASF) is used to lower the surface tension of oil–water interface in oil–water emulsions, Gulutaraldehyde (40%, Sigma Aldrich) was chosen as a cross-linking agent of PVA, and deionized water as a solvent. All materials were used as received. LCs are encapsulated by micro-channel emulsification method [29].

2.2. Optically isotropic LC mixtures.

We used MLC-2053 ($\Delta\varepsilon$ = 46.2 at 1 kHz, T_{NI} = 86 °C, n_{e} = 1.7472, n_{o} = 1.5122, Δn = 0.235 at 589 nm, K_{11} = 13.2 pN, K_{22} = 6.5 pN, K_{33} = 18.3 pN, γ_1 = 123 mPa·s, Merck Advanced Technologies Co., Ltd.) as a nematic LC, trimethylolpropane triacrylate (TMPTA, n_p = 1.473 at 589 nm, T_{g} = 62 °C, Sigma Aldrich), pentaerythritol tetraacrylate (PETTA, n_p = 1.484 at 589 nm, T_{g} = 65 °C, Sigma Aldrich) as host monomers (Figure S1), and 2-Methyl-4′-(methyl thio)-2-morpholinopropiophenone (Irgacure-907, excitation at 365 nm, Merck Advanced Technologies Co., Ltd.) as a photo-initiator (PI) for the initiation of radical photopolymerization in the composite upon the exposure of UV light. All materials were used as received. We basically reproduce the optically isotropic LC cell by following the fabrication process in the ref [6].

2.3. Cell process

The encapsulated LC mixtures were blade-coated on a glass substrate with patterned interdigitated indium-tin-oxide (ITO) electrode (electrode width w = 4 μm and space l = 4 μm). After drying water, the cell was baked at 90 °C for 1 h. The optically isotropic LC mixture was injected into a cell at 90 °C by capillary action. The cell was fabricated by sandwiching one glass substrate onto the other glass substrate with patterned ITO electrode (w = l = 4 μm) with the cell gap d. All cells were tested under a polarized optical microscope (POM) to observe the homogeneity of the mixture to clarify the optically isotropic property before and after UV curing. All cells were irradiated under UV with intensity of 140 mW/cm^2 for 8 min. All cells were prepared by following above condition unless otherwise mentioned.

2.4. Characterizations

We used a particle size analyzer (ELSZ-2000 series, Otsuka Electronics Co.,Ltd.) to analyze the size of the capsules. A POM (Eclipse E600, Nikon) was used for optical images taken by a CCD camera (DXM 1200, Nikon). The electro-optical properties were measured by a photodetector (DET36A/M, 350 – 1100 nm, Thorlabs), a function generator (33521A, Agilent), an oscilloscope (DPO 2024B, Tektronix), and He-Ne laser light (633 nm). Cells were placed in between crossed polarizers where longer-electrode axis was 45° to the polarization directions. To investigate the surface morphology of the polymer matrix, cells were soaked in n-hexane for a day to remove LCs from polymer matrix. The PVA polymer film was then coated with a conductive gold layer by RF sputtering to avoid the charge accumulation and then observation was done by a field emission scanning electron microscope (FESEM, SUPRA40VP, Carl Zeiss) installed in the Center for University-wide Research Facilities (CURF) at Jeonbuk National University. The post image processing was done by an open-source software (*ImageJ*, NIH). We fabricate submicron thin layers of both encapsulated LC and optically isotropic LC and removed LCs to acquire the polymer matrices. After taking FESEM images of the two cases, we analyze the average and standard deviation of cavities. We then analyze the areal filling factors (Figure S3).

3. Results and discussion

The schematic of LC encapsulation in PVA-dissolved water shows the LC director and the PVA shell in Fig. 1a. The fabricated LC-PVA encapsulation solution is shown in Fig. 1b. As the solution shows a white (in a brown vial) light scattering state, the measured diameter distribution of capsules is 565 ± 122 nm as shown in Fig. 1c. The blade-coating process is described in Fig. 1d-g that show the optical status of the mixture on a substrate. On a patterned-ITO glass substrate, we blade-coat the loaded encapsulated LC solution in room temperature as the white light scattering occurs right after the coating (Fig. 1e). The thin film of the solution is then kept in ambient air until water is all evaporated and the light scattering vanishes (Fig. 1f), which proves that LCs are well encapsulated in PVA without water. The substrate is then baked in the oven at 90 °C for 1 h. After the baking is done, the film shows excellent transparency as shown in Fig. 1g. The transparency implies the size of the capsule coated on the substrate is below the visible wavelength. We believe the size of the capsules is shrunk after water is dried away and polymerization of PVA.

To verify the size of the encapsulation, we observe the polymer matrix after removal of LCs in both the encapsulated LC and optically isotropic LC in Fig. 2. To verify more clear images of cavities in the polymer matrix, we fabricate submicron thickness $d \sim 0.7$ 8 μm with a single substrate for the encapsulated LC (Fig. 2a,b) and double substrates for the optically isotropic LC (Fig. 2c,d). The relatively uneven upper surface of the polymer matrix in Fig. 2a tells us which the dehydration and polymerization process is done without the upper substrate. The observed cavity size distribution is analyzed as the diameter is 379 ± 160 nm from Fig. 2b and 141 ± 55 nm from Fig. 2d. We also analyze the areal filling factor as 67.8% from Fig. 2b and 40.5% from Fig. 2d. (See Experimental Section for details) The results clearly show more than 27.3%. higher areal filling factor of the encapsulated LC than the optically isotropic LC, and the size of cavities in the encapsulated LC is ~ 2.7 times higher than that in the optically isotropic LC.

We observe the electro-optic properties of the encapsulated LC and compare the result with an optically isotropic LC as shown in Fig. 3. The POM images show a complete dark state of the encapsulated LC in between crossed polarizers. No scattering is observed in the dark states, which tells us the cavity size of the encapsulated LC and the optically isotropic LC is below the visible wavelength (Fig. 3ab). Upon applying voltage, LCs reorient into the electric field direction and consequently birefringence is induced owing to the Kerr effect as shown in Equation (1). We note that granular-like domains are observed upon the applied field in the encapsulated LC, which occurs owing to the topless coating process. The size is below the spatial resolving power of human eyes so it may not be an issue but controlling the time between drying and thermal polymerization may help to reduce the roughness in the encapsulated LC.

The electric field-dependent transmittance curve of the encapsulated LC shows threshold electric field E_{th} = 1.4 V/μm and driving electric field E_{op} = 4.6 V/μm, which are 30% and 46% lower than those of the optically isotropic LCs (E_{th} = 2.0 V/μm and E_{op} = 8.5 V/μm). In optically isotropic LC, on the other hand, there is residual birefringence as shown in the voltage-off state in Fig. 3b as the POM image is taken after a few cycles of field-driving up to 8.5 V/μm. As shown in Fig. 3c, we apply the voltage until the curve reaches the plateau in the voltage-dependent transmittance curve and almost no hysteresis is clearly observed in the encapsulated LC. To evaluate the hysteresis, we determine $H = (E_{asc} - E_{des}) / E_p \times 100\%$, where Ep is the electric field strength at peak transmittance, and Easc and Edes respectively are half of the peak when the voltage is ramping up and down. From Fig. 3b, we calculate H = 0.43% and 7.06% in the encapsulated LC and optically isotropic LC, respectively. It clearly tells us the hysteresis-free behavior in the encapsulated LC.

The measured refractive index changes are depicted in Fig. 3d. The dotted-straight lines are calculated from Equation (1), which represent quadratic field response of the induced birefringence. As the measured values with solid circles, however, are out of the tendency of the induced birefringence line, we calculate the fitting curves along the measured values with extended Kerr effect, which is governed by Equation (3). The measured values and the fitting curves seem to be in a good agreement; besides some small deviation that might be caused by the white light we used for the light source in the measurement, which covers the range of the visible wavelength (400 nm < λ < 650 nm). As explained in the Introduction, the induced-refractive-index change δn is smaller than the refractive index of the host LCs (Δn = 0.235 and 0.240, respectively). We measure $\delta n \sim 0.028$ at $E \sim 6.26$ V/μm and $\delta n \sim 0.054$ at $E \sim 2.60$ V/μm in the optically isotropic LC and the encapsulated LC, respectively. The results show that the encapsulated LC shows almost 1.7 times higher δn at 2.4 times lower E than the optically isotropic LC. However, the acquired δn_{sat} is ~ 17% less in the optically isotropic LC and 2.5% less in the encapsulated LC than the ideal case (Δn_{ind} / 3) even though we consider the filling factors and the factor of 1/3 from Equation (2). We note that the 17% and 2.5% are big difference. We can clearly explain this tendency

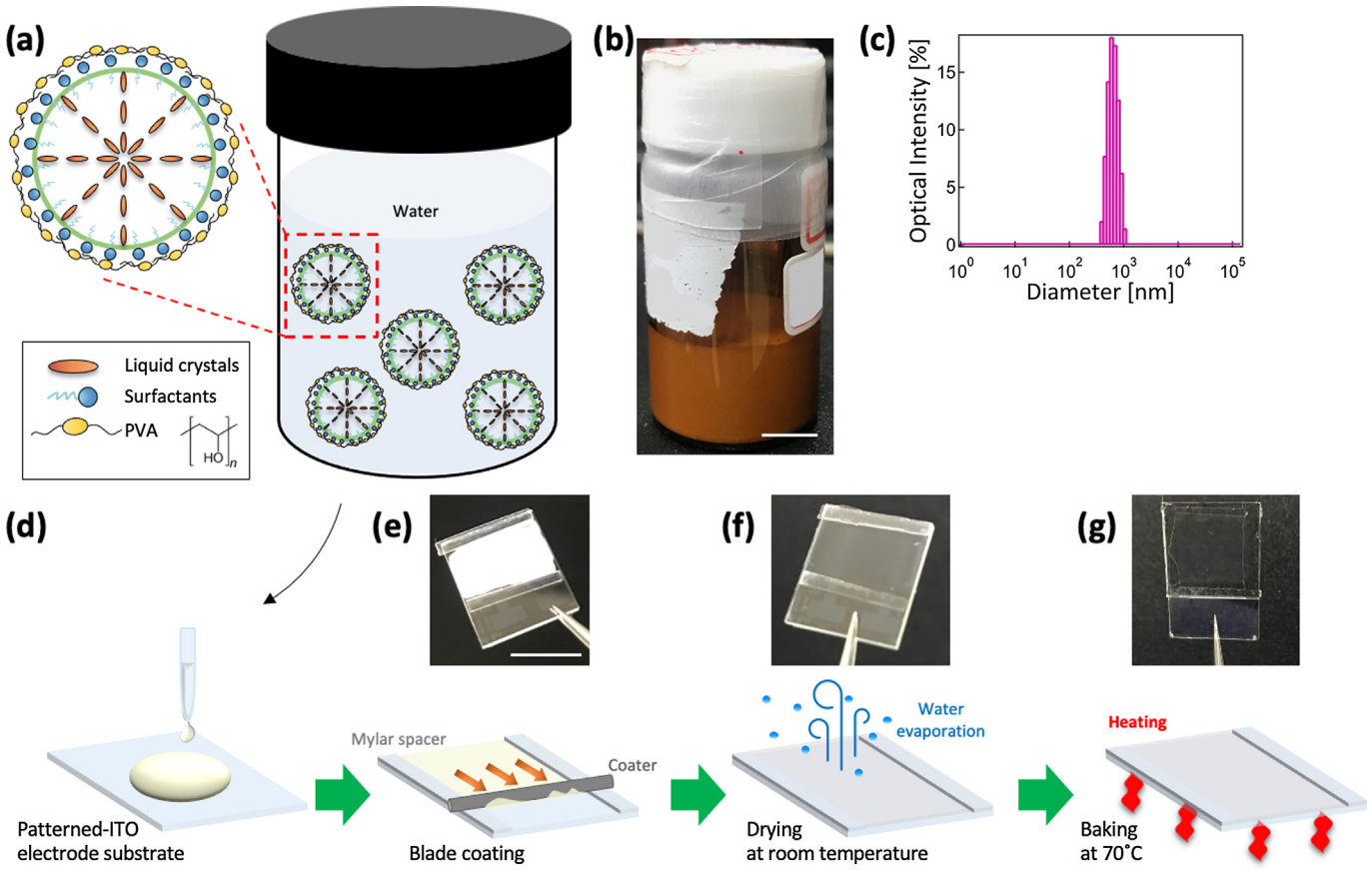

Fig. 1. Encapsulation and a unit cell fabrication process. **(a)** Schematic representation of encapsulated LCs. **(b)** The LC encapsulated mixture in a brown vial. The scale bar is 1 cm. **(c)** The dynamic light scattering shows a peak with the diameter of 565 ± 122 nm when analyzing a particle size analyzer (Table S1). **(d-g)** Schematics of the fabrication process: (d) the mixture dropped on a patterned-ITO substrate, (e) blade coating, (f) drying, (g) baking. Insets in (e-g) show the mixture on a substrate at each step. The scale bar is 1 cm.

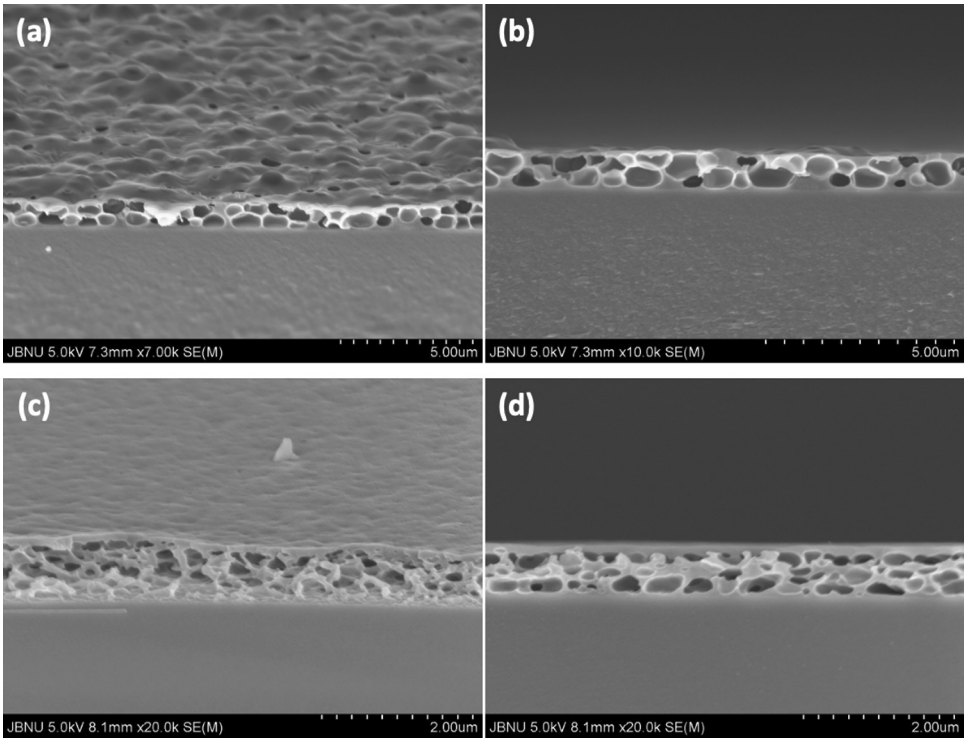

Fig. 2. Field-emission scanning electron microscope (FE-SEM) images of the polymer matrices of **(a,b)** the encapsulated LC and **(c,d)** optically isotropic LC.

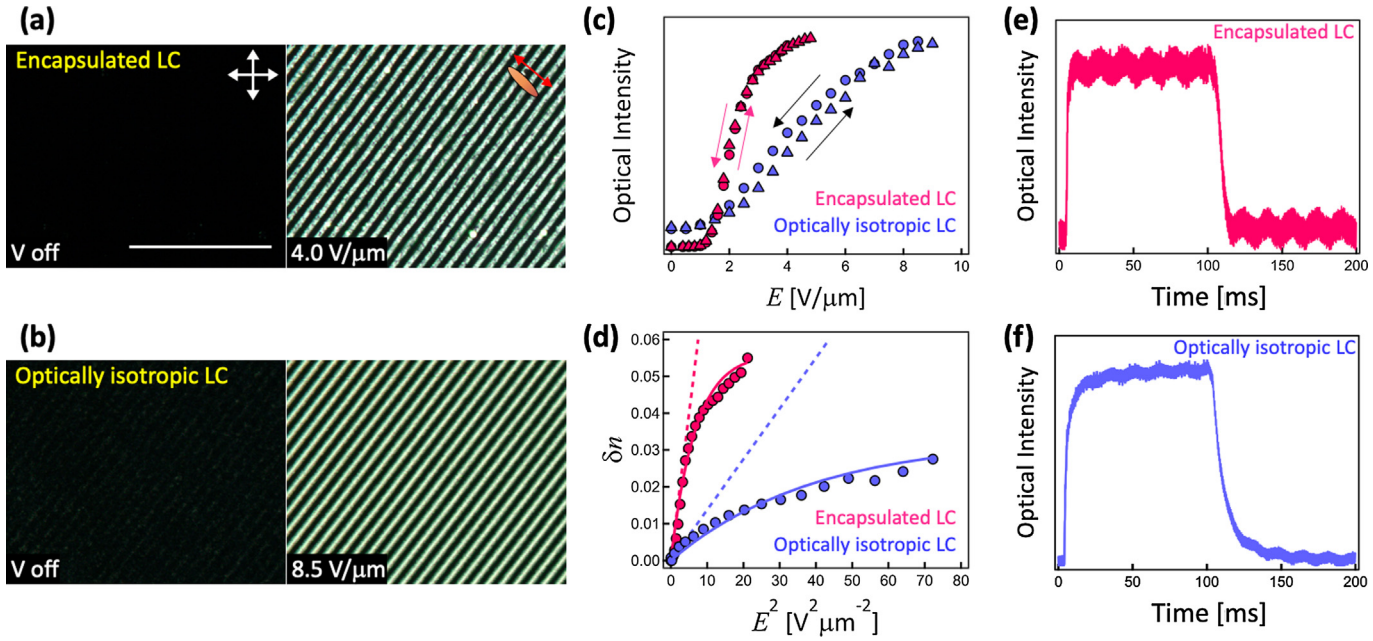

Fig. 3. The electro-optical properties of the encapsulated LC and optically isotropic LC. **(a,b)** Polarized optical microscopy (POM) images of (a) the encapsulated LC cell and (b) optically isotropic LC cell as ramping up electric field strength. The white arrows represent the optic axes of crossed polarizers. The red-double headed arrow and rod indicate the direction of the electric field and induced birefringence. The scale bar is 100 μm. **(c)** Measured electric field-dependent transmittances. The red and blue arrows represent when ascending and descending the electric fields. **(d)** The measured refractive index change (circles), linear lines with Equation (1) (dotted-straight lines), and the extended Kerr effect with Equation (3) (magenta-convergent lines). **(e,f)** The time-dependent transmittance of (e) the encapsulated LC and (f) the optically isotropic LC. (For interpretation of the references to color in this figure legend, the reader is referred to the web version of this article.)

by the different LC filling factors in the polymer matrices (40.5% and 67.8% in the optically isotropic and encapsulated LCs) even if the difference in Δn of the host LCs in each mode is slight.

We also evaluate the response time and analyze it from the time-dependent transmittance measurements as shown in Fig. 3e,f. The measurement gives the response times τ_{on} (τ_{off}) = 0.5 (2.2) ms in the encapsulated LC when applying 4 V/μm, and τ_{on} (τ_{off}) = 3.3 (10.3) ms in the optically isotropic LC when applying 8.5 V/μm. This shows the fast response time in the encapsulated LC. As the hysteresis analysis tells us there is residual birefringence upon the applied electric fields, the relaxation of LCs is slow in the optically isotropic LCs. The hysteresis-free response contributes to the fast response of LC in the encapsulated LC composite system. As all the estimated, calculated, and measured physical values are summarized in Table 1, the encapsulated LC shows greatly improved K_r, with high F, and fast response time with minor hysteresis.

4. Conclusion

In this work, we fabricate a highly filled LC-polymer composite film by oil-in-water encapsulation method. By using this method, the filling factor can be increased because the LC capsules are closely packed. We have achieved high LC filling factor by 67.8% in the encapsulated LC, compared to of 40.5% in the conventional optically isotropic LC. We measure the threshold and the operating electric fields of the encapsulated LC (E_{th} = 1.4 V/μm and E_{op} = 4.6 V/μm), which are relatively lower than those in the optically isotropic LC (E_{th} = 2.0 V/μm and E_{op} = 8.5 V/μm). We also measure the response times of the encapsulated LC, τ_{on} (τ_{off}) = 0.5 (2.2) ms, which are much faster than those in the optically isotropic LC, τ_{on} (τ_{off}) = 3.3 (10.3) ms. We can confirm that the highly filled LC-polymer composite system shows low-operating voltage, fast-response time, and hysteresis-free in electro-optic field responses. With the proposed LC encapsulation method, superior electro-

Table 1
Encapsulated LC (ELC), optically isotropic LC (OILC), the concentration of LC in composites c_{LC}, the areal filling factor F, the cavity size D, saturated refractive index change δn_{sat}, saturated electric field strength E_{sat}, threshold electric field E_{th}, operating electric field E_{op}, Kerr constant K_r, response times τ_{on}, τ_{off}, and hysteresis H.

Sample names	Polymer	c_{LC} [%]	F [%]	D [nm]	δn (E) [V/μm]	E_{th} (E_{op}) [V/μm]	K_r [nm/V^2]	τ_{on} [ms]	τ_{off} [ms]	H [%]
ELC	PVA	70	67.8	379 ±160	0.054 (2.6)	1.4 (4.6)	14.50	0.5	2.2	0.43
OILC	PETTA TMPTA	42	40.5	141 ±55	0.028 (6.3)	2.0 (8.5)	2.50	3.3	10.3	7.06
OILC[a]	NOA65	42	–	–	–	1.6 (9.0)	2.66	0.8	2.3	0.40

[a] from the reference [6].

optic properties can be achieved as demonstrated in the experiments. We believe this study can provide us an efficient solution to realize free-form flexible LC displays and compact tunable photonic systems with low power.

CRediT authorship contribution statement

Seok Lyul Lee: Methodology, Writing – review & editing. **MinSu Kim:** Methodology, Formal analysis, Writing – original draft, Writing – review & editing, Supervision, Funding acquisition. **DaYeon Lee:** Methodology, Investigation. **Yi-Hsin Lin:** Writing – review & editing. **Seung Hee Lee:** Conceptualization, Supervision, Funding acquisition.

Declaration of Competing Interest

The authors declare that they have no known competing financial interests or personal relationships that could have appeared to influence the work reported in this paper.

Acknowledgments

This work was supported by the Basic Science Research Program through the National Research Foundation, Korea (NRF) funded by the Ministry of Education [2021R1I1A1A01060001]; by the Regional Leading Research Center Program through the National Research Foundation (NRF), Korea, funded by the Ministry of Science and ICT, Korea [2019R1A5A8080326]; and by ITECH R&D Program of MOTIE/KEIT (Ministry of Trade, Industry & Energy / Korea Evaluation Institute of Industrial Technology) [20012555] and [20016808].

Appendix A. Supplementary material

Supplementary data to this article can be found online at https://doi.org/10.1016/j.molliq.2022.119254.

References

[1] M. Noda, N. Kobayashi, M. Katsuhara, A. Yumoto, S. Ushikura, R. Yasuda, N. Hirai, G. Yukawa, I. Yagi, K. Nomoto, T. Urabe, An OTFT-driven rollable OLED display, J. Soc. Inf. Disp. 19 (2011) 316–322, https://doi.org/10.1889/JSID19.4.316.
[2] L.Y. Lin, C.C. Cheng, C.Y. Liu, M.F. Chiang, P.H. Wu, M.T. Lee, C.Y. Chen, C.C. Chan, C.C. Lin, C.H. Chang, 20.2L: Late-News Paper: A 4-inch QVGA Flexible AMOLED Driven by Solution-Processed Metal Oxide TFTs, SID Symp. Dig. Tech. Pap. 45 (2014) 252–255, doi:10.1002/J.2168-0159.2014.TB00069.X.
[3] R.A. Chipman, W.-S.-T. Lam, G. Young, Polarized Light and Optical Systems, Polariz. Light Opt. Syst. (2018), https://doi.org/10.1201/9781351129121.
[4] H.-C. Lin, M.-L. Lee, P.-L. Chen, Y.-H. Lin, Y.-J. Wang, Optical measurement in a curved optical medium with optical birefringence and anisotropic absorption, Opt. Express, Vol. 29, Issue 23, 29 (2021) 38654–38668, doi:10.1364/OE.439521.
[5] S. Pagidi, R. Manda, H.S. Shin, J. Lee, Y.J. Lim, M.S. Kim, S.H. Lee, Enhanced electro-optic characteristics of polymer-dispersed nano-sized liquid crystal droplets utilizing PEDOT:PSS polymer composite, J. Mol. Liq. 322 (2021), https://doi.org/10.1016/J.MOLLIQ.2020.114959 114959.
[6] N.H. Park, S.C. Noh, P. Nayek, M.H. Lee, M.S. Kim, L.C. Chien, J.H. Lee, B.K. Kim, S. H. Lee, Optically isotropic liquid crystal mixtures and their application to high-performance liquid crystal devices 42 (2015) 530–536, https://doi.org/10.1080/02678292.2015.1006698.
[7] S. Bronnikov, S. Kostromin, V. Zuev, Polymer-Dispersed Liquid Crystals: Progress in Preparation, Investigation, and Application 52 (2013) 1718–1735, https://doi.org/10.1080/00222348.2013.808926.
[8] S. Pagidi, H.S. Park, D.Y. Lee, M.S. Kim, S.H. Lee, Nanosize-confined nematic liquid crystals at slippery interfaces of polymer composites consisting of poly (hexyl methacrylate), J. Mol. Liq. (2022), https://doi.org/10.1016/J.MOLLIQ.2022.118540 118540.
[9] J. Kerr, XL. A new relation between electricity and light: Dielectrified media birefringent, Lond. Edinb. Dublin philos. 50 (1875), 337-348, doi:10.1080/14786447508641302.
[10] H. Kikuchi, M. Yokota, Y. Hisakado, H. Yang, T. Kajiyama, Polymer-stabilized liquid crystal blue phases, Nat. Mater. 2002 11. 1 (2002) 64–68, doi:10.1038/nmat712.
[11] J. Yan, H.C. Cheng, S. Gauza, Y. Li, M. Jiao, L. Rao, S.T. Wu, Extended Kerr effect of polymer-stabilized blue-phase liquid crystals, Appl. Phys. Lett. 96 (2010), https://doi.org/10.1063/1.3318288 071105.
[12] L. Rao, Z. Ge, S.T. Wu, S.H. Lee, Low voltage blue-phase liquid crystal displays, Appl. Phys. Lett. 95 (2009), https://doi.org/10.1063/1.3271771 231101.
[13] M. Kim, M.S. Kim, B.G. Kang, M.K. Kim, S. Yoon, S.H. Lee, Z. Ge, L. Rao, S. Gauza, S.T. Wu, Wall-shaped electrodes for reducing the operation voltage of polymer-stabilized blue phase liquid crystal displays, J. Phys. D. Appl. Phys. 42 (2009), https://doi.org/10.1088/0022-3727/42/23/235502 235502.
[14] M.S. Kim, M. Kim, J.H. Jung, K.S. Ha, S. Yoon, E.G. Song, A.K. Srivastava, S.-W. Choi, G.-D. Lee, S.H. Lee, P-132: Blue Phases Liquid Crystal Cell Driven by Strong In-Plane Electric Field, SID Symp. Dig. Tech. Pap. 40 (2009) 1615, https://doi.org/10.1889/1.3256629.
[15] S. Yoon, M. Kim, M.S. Kim, B. Gyun Kang, M.-K. Kim, A. Kumar Srivastava, S. Hee Lee, Z. Ge, L. Rao, S. Gauza, S.-T. Wu, Optimisation of electrode structure to improve the electro-optic characteristics of liquid crystal display based on the Kerr effect, Liq. Cryst. 37 (2010) 201–208, https://doi.org/10.1080/02678290903494601.
[16] M.K. Kim, M.S. Kim, B.G. Kang, G.H. Yang, A. Mukherjee, S.W. Kang, H. Lee, S.T. Shin, S.H. Lee, Maximization of an Electric Field Penetrating an Optically Isotropic Phase Liquid Crystal for Low Operating Voltage Display, 543 (2011) 194/[960]-199/[965], doi:10.1080/15421406.2011.569525.
[17] N.H. Park, S.I. Park, K.D. Suh, A novel method for encapsulation of a liquid crystal in monodisperse micron-sized polymer particles, Colloid Polym. Sci. 279 (2001) 1082–1089, https://doi.org/10.1007/S003960100524.
[18] M.S. Kim, L.C. Chien, Topology-mediated electro-optical behaviour of a wide-temperature liquid crystalline amorphous blue phase, Soft Matter. 11 (2015) 8013–8018, https://doi.org/10.1039/c5sm01918d.
[19] M.S. Kim, Liquid Crystalline Amorphous Blue Phase: Tangled Topological Defects, Polymer-stabilization, and Device Application. Doctoral dissertation, Kent State University, (2015). http://rave.ohiolink.edu/etdc/view?acc_num=kent1448894363.
[20] M.S. Kim, L.-C. Chien, Enhanced stability, hysteresis, and dark state of polymer-stabilized blue phase III, SID Symp. Dig. Tech, Pap, 2015.
[21] M.S. Kim, R.K. Mishra, R. Manda, G. Murali, T.-H. Kim, M.-H. Lee, M. Yun, S. Kundu, B.-S. Kim, S.H. Lee, Reduced graphene oxide (RGO) enriched polymer network for highly-enhanced electro-optic performance of a liquid crystalline blue phase, RSC Adv. 7 (2017) 16650–16654, https://doi.org/10.1039/C6RA28465E.
[22] R. Manda, S. Pagidi, Y. Heo, Y.J. Lim, M.S. Kim, S.H. Lee, Electrically tunable photonic band gap structure in monodomain blue-phase liquid crystals, NPG Asia Mater. 2020 121. 12 (2020) 1–9, doi:10.1038/s41427-020-0225-8.
[23] P.R. Gerber, Electro-Optical Effects of a Small-Pitch Blue-Phase System 116 (2011) 197–206, https://doi.org/10.1080/00268948508074573.
[24] L. Pschyklenk, T. Wagner, A. Lorenz, P. Kaul, Optical Gas Sensing with Encapsulated Chiral-Nematic Liquid Crystals, ACS Appl. Polym. Mater. 2 (2020) 1925–1932, https://doi.org/10.1021/ACSAPM.0C00142/SUPPL_FILE/AP0C00142_SI_001.PDF.
[25] S.S. Gandhi, M.S. Kim, J.-Y. Hwang, L.-C. Chien, Electro-optical Memory of a Nanoengineered Amorphous Blue-Phase-III Polymer Scaffold, Adv. Mater. (2016) 1–8, https://doi.org/10.1002/adma.201603226.
[26] T. Hirose, A. Yoshizawa, Comparison of electro-optical switching between polymer-stabilised cubic and amorphous blue phases 42 (2015) 1290–1297, https://doi.org/10.1080/02678292.2015.1048755.
[27] J.A. Martínez-González, X. Li, M. Sadati, Y. Zhou, R. Zhang, P.F. Nealey, J.J. De Pablo, Directed self-assembly of liquid crystalline blue-phases into ideal single-crystals, Nat. Commun. 8 (2017) 15854, https://doi.org/10.1038/ncomms15854.
[28] R. Manda, S. Pagidi, Y.J. Heo, Y.J. Lim, M.S. Kim, S.H. Lee, Polymer-Stabilized Monodomain Blue Phase Diffraction Grating, Adv. Mater. Interfaces. 7 (2020) 1901923, https://doi.org/10.1002/ADMI.201901923.
[29] I. Kobayashi, M. Nakajima, K. Chun, Y. Kikuchi, H. Fujita, Silicon array of elongated through-holes for monodisperse emulsion droplets, AIChE J. 48 (2002) 1639–1644, https://doi.org/10.1002/AIC.690480807.